Available online at www.sciencedirect.com

SciVerse ScienceDirect

Ceramics International 38 (2012) 6181–6189

CERAMICS INTERNATIONAL

www.elsevier.com/locate/ceramint

Influence of hydroxyapatite pore geometry on tigecycline release kinetics

Božana Čolović[a], Snežana Pašalić[b], Vukoman Jokanović[a,*]

[a]*Institute of Nuclear Sciences "Vinča", Laboratory for Radiation Chemistry and Physics, Mike Petrovića Alasa 12-14, University of Belgrade, Belgrade 11001, Republic of Serbia*

[b]*Ministry of Education and Science, Njegoševa 12, Belgrade 11000, Republic of Serbia*

Received 10 June 2011; received in revised form 17 April 2012; accepted 23 April 2012
Available online 14 May 2012

Abstract

Calcium hydroxyapatite (CHA), as one of the most important ceramic materials in bone tissue engineering, was used as a delivery system for tigecycline, a potential antibiotic in treatment of osteomyelitis. Tigecycline, in a solid state, was mixed with CHA powder and the obtained mixture was compressed into tablets. The release of tigecycline from these tablets in a pH 7.4 phosphate-buffered saline solution was measured by a UV–vis spectrophotometer at 37 °C. The total dose of tigecycline was released for 5 to 30 days, depending on the applied pressure and drug concentration. A new drug release mechanism that determines the relationship between pore sizes and drug release rate is proposed. It explains and quantifies the drug release kinetics based on pore sizes and pore size distribution.

Keywords: B: Pore geometry; E: Hydroxyapatite; Multilevel carrier; Drug release

1. Introduction

Calcium hydroxyapatite is one of the most employed ceramics in bone tissue engineering. CHA scaffolds have been widely used as implants in dentistry and orthopedics due to their biocompatibility with bone tissue and osteoconductivity [1,2]. Also, CHA is able to absorb different chemical species on its surface which makes it a suitable candidate for drug delivery systems [3,4]. Antibiotic administration at the surgical site to prevent bacterial infections, occurring frequently, is of great importance in bone graft surgery. Prosthetic joint infections represent the most devastating complication, with high morbidity and substantial cost [5,6]. The conventional route of antibiotic administration results in low antibiotic level in the skeletal tissue caused by reduced blood circulation in this tissue or limited antibiotic penetration to the bone [7]. So, by entrapping the antibiotic into an apatite scaffold, high local concentrations of antibiotic can be achieved. Antibiotic release from the scaffold ensures protection from bacterial infections over a long postoperative period, which may last for a few days up to several weeks, although some authors conceive that antibiotics should be administrated no longer than twenty-four hours after the surgical intervention. On the other hand, the rest of body is protected against high antibiotic concentrations by blood-bone barrier [6,8,9]. Apatite plays a double role here, as a bone substitute material and as a drug delivery device, because it fills the bone defect and also provides desirable drug concentration at the surgical site.

There are many bone infections caused by multi-resistant Gram-positive and Gram-negative organisms, so new antimicrobials are needed to repress these resistant bacteria. Antibiotic treatment of osteomyelitis, caused by methicillin resistant *Staphylococcus aureus*, is especially interesting. These infections are very difficult to treat and therapeutic options are limited [10,11]. Therefore, a new class of antibiotics, glycylcycline antibiotics, has been developed to overcome the resistance to tetracyclines. They are active against many resistant pathogens by inhibiting bacterial protein synthesis. Best known among them is tigecycline,

*Corresponding author. Tel.: +38 1113408724; fax: +38 1113408607.
E-mail address: vukoman@vinca.rs (V. Jokanović).

0272-8842/$36.00
http://dx.doi.org/10.1016/j.ceramint.2012.04.069

a 9-t-butylglycylamido synthetic derivative of minocycline, which is currently licensed for the treatment of complicated skin and soft tissue infections, as well as complicated intra-abdominal infections. The use of tigecycline for the treatment of bone diseases, however, has not been studied enough due to lack of information on their disposition, but it seems to be a potential drug in treatment of severe orthopedic infections [12,13]. Several studies have shown the efficacy of tigecycline in a variety of animal infection models for osteomyelitis, endocarditis, pneumonia and peritonitis. In humans, tigecycline is widely distributed in the body, but some studies have shown that its concentration in bone is relatively low when compared to serum. One study on humans has shown that tigecycline may be used in treatment of chronic osteomyelitis resistant *Acinetobacter sp.* [10].

Drug release kinetics from apatite cements has not been completely clarified yet. Many models have been proposed [1,14–16] but none of them describes the whole kinetics of release. The process has been considered by many authors as a surface phenomenon. Accordingly, the kinetics of drug release at the initial stage is controlled by surface phenomenon, while that of sustained release depends on the penetration depth determined by the cement porosity. Thus, the release kinetics is related to the number and the size of pores in the cement used [17–20].

2. Materials and methods

2.1. Materials

The apatite powder obtained hydrothermally was used in this study. Powders of calcium oxide (CaO) from eggshells and $(NH_4)_2HPO_4$ (p.a., Merck) were used for hydrothermal synthesis of CHA. The chicken eggshells were calcined at 900 °C, till complete carbon removal (dissociation of $CaCO_3$ to CaO). First, two precursors were prepared: (i) 500 ml of 3.02 cmol aqueous suspension of $Ca(OH)_2$ and (ii) 500 ml of 2.32 cmol aqueous solution of $(NH_4)_2HPO_4$. Then, the $(NH_4)_2HPO_4$ solution was poured into the $Ca(OH)_2$ suspension and vigorously stirred. The pH of the so-prepared solution mixture was adjusted to 7.4 by adding 0.1 M HCl or $(NH_4)OH$. Finally, this mixture was transferred into a beaker, covered with a glass plate, and autoclaved at a temperature of 150 °C and pressure of 5 bar for 8 h. After hydrothermal treatment in the autoclave, the precipitate was decanted, dried at 80 °C for 48 h, ground, washed with deionized water, and ultracentrifuged in order to obtain the purest possible CHA [21].

2.2. Fabrication of tablets

Tigecycline, in different concentrations (1, 2, 3 and 5% w/w), was mixed with CHA powder and compressed into tablets with a pressure of 16 and 160 MPa using a hydraulic press. Tablet parameters were: diameter: 10 mm and height: 2 mm.

2.3. Tablet evaluation

XRD: An X-ray diffraction (XRD) method (Philips PW 1050) with Cu-Kα1–2 radiation was used for phase analysis of CHA and determination of crystallite sizes and lattice parameters. Data were analyzed in the range of 2θ from 9 to 67° with a scanning step of 5°, and exposition time of 2 s per step [21].

IR: A PERKIN ELMER 983G IR spectrometer, with KBr pastille, was used for CHA powder characterization. IR spectra were recorded in the wave number range 4000–400 cm^{-1}.

SEM: A scanning electron microscope (SEM JEOL 5300) was used to analyze the morphology and size distribution of CHA particles. Samples for SEM analysis were prepared as follows: they were suspended in ethanol and dispersed by ultrasound for 10 min, and then coated with gold by the PVD process.

SBET: Specific surface areas were measured by nitrogen adsorption at −96 °C using a Varian Aerograph (model 920) gas chromatograph equipped with TCD detector. The instrument is highly sensitive and provides measurements of surface areas as low as 0.1 m^2 in a sample cell. Before the measurements, the samples were treated at 150 °C in a helium flow for 2 h. After that, a gas mixture of 27 vol% of nitrogen in helium (30 cm^3/min) was passed over the sample and the sample cell was cooled by immersion in liquid nitrogen. The cooling sample adsorbed a certain amount of nitrogen from the gas stream until adsorption equilibrium was established. After removal of the liquid nitrogen bath, the sample was warmed and the adsorbed nitrogen released, enriching the effluent monitored by a TCD detector. When desorption was complete, a known volume of nitrogen (0.5 cm^3) was added to the nitrogen–helium stream. By comparing desorption and calibration peaks, the volume of nitrogen adsorbed by the sample was calculated and the surface area of the sample determined by "one point" BET method. The assumption that the synthesized particles were spheroids enabled the calculation of the average radius of particles ($dBET = 6/\rho Sw$), where Sw is the specific surface area and $\rho = 3.156$ g/cm^3 is the theoretical density of synthesized CHA powders.

Porosimetry: Porosimetry measurements were carried out on a Carlo Erba Porosimeter 2000 using the Milestone 200 Software System. This high-pressure mercury intrusion porosimeter operates in the interval 0.1–200 MPa, enabling estimation of pores in the range from 7.5 to 15000 nm.

2.4. Drug release

Tigecycline release was measured after immersion of tablets into 40 ml phosphate buffer saline (PBS) at 37 °C and continuous stirring. The quantity of released antibiotic was measured using a UV–vis spectrophotometer at the wavelength of 245 nm, by taking 3 ml samples at desired time intervals. Withdrawn samples were replaced with fresh 3 ml PBS to simulate physiological conditions.

2.5. Drug release kinetics—general approach

Drug release kinetics depends on the microstructure of the drug delivery device used, drug solubility, type of bond between the drug and the device, and, if the device degrades, on the mechanism of its degradation [1,22–24]. Although resorbable, calcium phosphate cements can be treated as non-biodegradable devices because the rate of drug liberation is much higher than the rate of matrix degradation. So, we can say that they are diffusion-controlled devices, where drug release is controlled by the diffusion process through the cement device.

Equations for drug release from diffusion controlled devices are based on Fick's second diffusion law. A well-known is Higuchi's equation, based on a pseudo steady-state approach, which can describe, at least, the initial phase of the release (about 60% of the total amount released):

$$M_t = A\sqrt{C_s(2C_0 - C_s)Dt}, \quad (1)$$

where M_t is the amount of drug released for time t; A is the surface area of the device; D is the diffusion coefficient of the drug in the matrix; C_s is the solubility of the drug in the matrix; C_0 is the initial concentration of the drug in the matrix [1,14,25].

When drug loading is equal to or less then saturation ($C_0 \leq C_s$), solutions to Fick's second law can be easily found, and the particular expression for semi-infinite geometry is:

$$M_t = 2AC_0\sqrt{\frac{Dt}{\pi}}, \quad (2)$$

which allows determination of diffusion coefficient [25].

The Korsmeyer–Peppas model is also used to describe the drug release kinetics [15]. This equation is more general than Higuchi's and it is applicable to degrading matrices in which the drug release mechanism often deviates from Fick's law and follows an anomalous behavior described by the following equation:

$$M_t/M_\infty = kt^n, \quad (3)$$

where M_t is the quantity of drug released at time t, M_∞ is the quantity of drug released at infinite time, k is the kinetic constant, while n is the release exponent (for cylindrical matrices n takes values from 0.43 to 0.5 when Fick's law is applicable (diffusion controlled release) and $0.50 < n < 1.0$ when Fick's law is not applicable (anomalous transport)). This law, too, is generally not applicable below $0.6(M_t/M_\infty)$ [15].

3. Results and discussion

3.1. Phase analysis

XRD: The obtained X-ray data (Fig. 1) shows that the hydrothermally synthesized powder corresponds to carbonated calcium hydroxyapatite $Ca_{10}(PO_4)_6(OH)_2$ (JCPDS 9-432). All characteristic diffraction patterns are present: (2 1 1) at $2\theta = 31.9°$; (1 1 2) at $2\theta = 32.26°$, (3 0 0) at $2\theta = 33.12°$, (0 0 2) at $2\theta = 25.86°$, (2 2 2) at $2\theta = 46.86°$, and (2 1 3) at $2\theta = 49.58°$ [20]. The size of crystallites, calculated using Sherer's equation, is 8–22 nm.

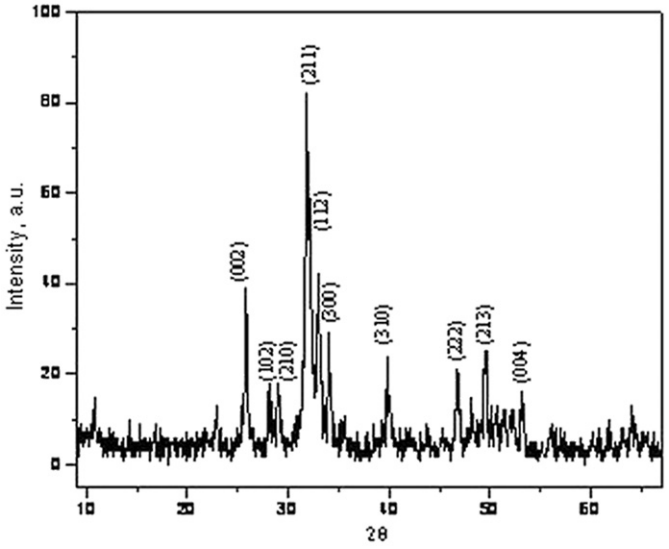

Fig. 1. X-ray diffraction pattern of hydrothermally synthesized CHA powder.

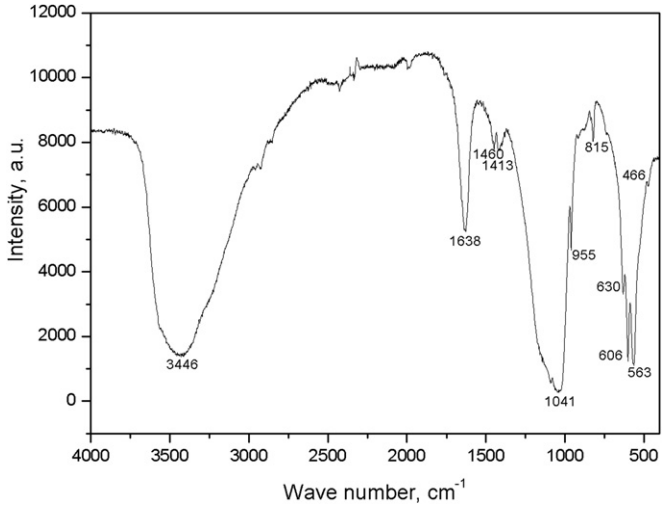

Fig. 2. IR spectrum of hydrothermally synthesized CHA powder.

IR: The IR spectrum of the synthesized CHA (Fig. 2) shows bands characteristic of hydroxyapatite. The asymmetric stretching ($\nu 3$) and bending ($\nu 4$) modes of PO_4^{3-} ion were detected at about 1092 and 1042 cm^{-1}, and 603 and 569 cm^{-1}, respectively; while symmetrical stretching modes (ν_1 and ν_2) of PO_4^{3-} ion were registered at around 957 and 473 cm^{-1}, respectively. The liberation and the stretching mode of OH^- were detected at around 630 and 1626 cm^{-1}, respectively. The stretching vibrations ascribed to CO_3^{2-} at about 1442, 1406 and 875 cm^{-1} are also present. This indicates incorporation of the carbonate group into the apatite structure. The band registered at

630 cm^{-1} is ascribed to the liberation mode of the OH^- vibration. It is evident that type B carbonated hydroxyapatite was obtained and that the replacements at the positions of the OH^- ions, revealed by changes in shape and position of the band at 3658 cm^{-1}, indicate that these changes were not predominantly caused by the substitution of OH^- by CO_3^{2-}.

3.2. SEM

SEM micrograph (Fig. 3) shows that the CHA powder consists of agglomerates, which are very similar in shape and size (1–5 μm). These agglomerates were built up from fine particles 200 nm in size. Agglomerate forms are irregular with oval edges due to spherical shapes of individual particles. [21].

3.3. SBET

Usually, the characteristics of porous structures are described according to the IUPAC pore size classification. Macropores are defined as pores larger than 50 nm, mesopores are typically in the range of 50–2 nm in size, whereas micropores correspond to pores smaller than 2 nm. Table 1.

The particle diameter, calculated from the specific surface area of CHA powder is 160 nm.

3.4. Porosimetry

Analyzing differential pore volume plot (Fig. 4), derivatives $dV/d(\log r)$ as a function of r, it is possible to completely define the pore distribution in the system. This function connects the pore diameter and partition of corresponding pores, for each discrete value of pore diameter.

Differential pore volume in the tablet compressed with the pressure of 16 MPa (tablet 1) is significantly higher than that in the tablet compressed with the pressure of 160 MPa (tablet 2), thus faster drug release is expected from tablet 1 (Fig. 4).

Pore size distribution and their partition to the total pore volume are given in a histogram (Fig. 5) for easier comparisons.

As can be seen in Fig. 5, pores of various sizes and partitions are present in the tablets. Multimodal distribution of pore sizes derives from different types of pores: the largest pores formed during tablet compression, large pores between aggregates, pores between particles, small pores between smaller particles arranged inside of the biggest agglomerates and the smallest pores between basic particles, which are in some cases on the level of crystallites inside of basic particles (basic particles are the smallest particles in the system whose sizes were determined by BET method, while the sizes of crystallites were determined by XRD). Comparing pore sizes in tablet 1

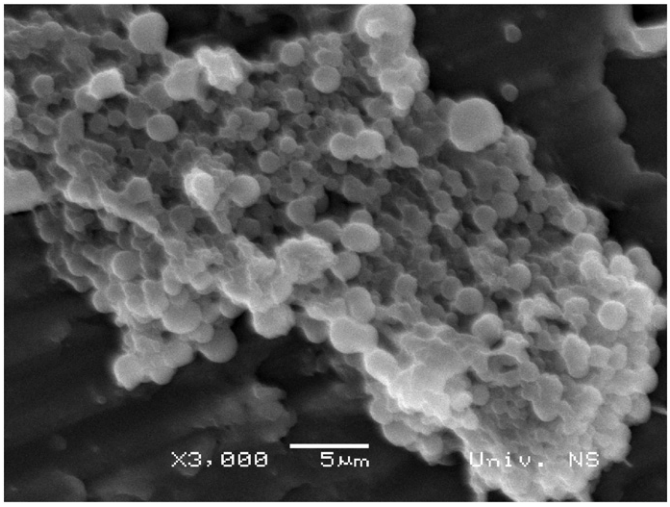

Fig. 3. SEM micrograph of CHA powder.

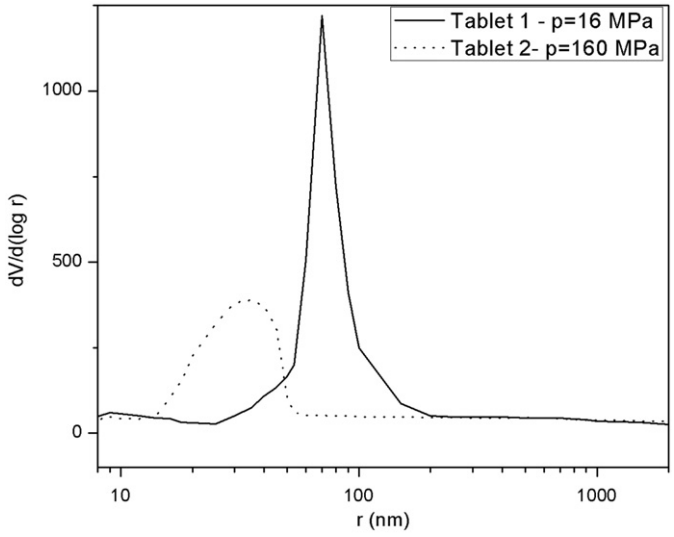

Fig. 4. Differential pore volume.

Table 1
Porosity parameters determined by BET method.

Sample	S_{BET}, m^2/g	Total pore volume, cm^3/g	Mean pore diameter size, nm	Portion of mesopores, %	Portion of macropores, %
CHA powder	12	1.00	310	10	90
Tablet 1, $p=16$ MPa	13	0.39	75	36	64
Tablet 2, $p=160$ MPa	11	0.17	35	65	35

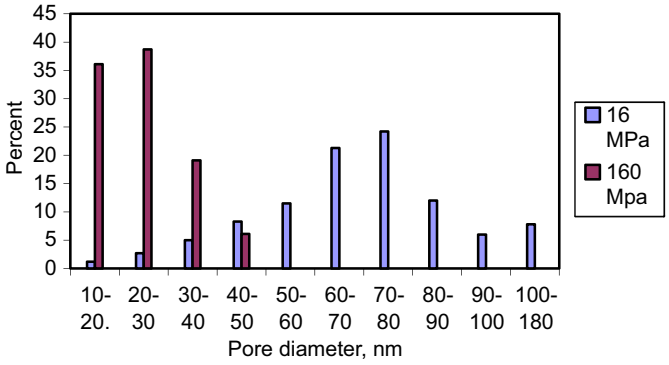

Fig. 5. Pore size distribution and their partition for tablets 1 and 2.

(p=16 MPa) and tablet 2 (p=160 MPa), it is evident that the pores in tablet pressed under p=160 MPa are significantly smaller. The presence of pores with diameters of 10–20 nm in tablet 2 is 36%, while in tablet 1 only 1.2%. The most dominant pores in tablet 2 are those with diameters of 20–30 nm, while in tablet 1 those with diameters of 60–80 nm.

3.5. Drug release from tablets

According to the curves given in Fig. 6, the drug release occurs in two stages. First stage is characterized by a fast initial release, and the second by a continuous slow release. High initial release rate is probably a result of drug solubility at the tablet surface [26].

We confirmed that Higuchi's equation can be applied to the experimental data only to the initial period of drug release (when 50%–67% of the total drug amount is released—for tablets compressed with the pressure of 16 MPa (tablets 1) or 30%–56%—for tablets compressed with the pressure 160 MPa (tablets 2)).

As it is shown, Higuchi's equation cannot be applied for processing of all experimental data. Therefore, the experimental data were firstly divided into several appropriate sets and the equation was successfully applied to each set separately. Each set is characterized by the corresponding drug release rate. This enables the determination of the effective diffusion coefficients, over direction coefficients estimated from corresponding data sets (data belonging to one linear segment of the curves given in Fig. 7), using Eq. (2).

Regarding all these segments, a quite good relationship between the drug release rate and corresponding pore sizes can be observed. Pores can be classified in three groups, for tablets 1: large (60–180 nm), medium (40–60 nm) and small (10–40 nm) and for the tablets 2: 20–50 nm, 15–20 nm and 10–15 nm. The obtained data showed that the percent of drug released within any linear segment was in agreement with the partition of corresponding group of pores in total pore volume. So, it was shown that the drug release occurred gradually, first from the biggest pores, then from the medium and finally from the smallest.

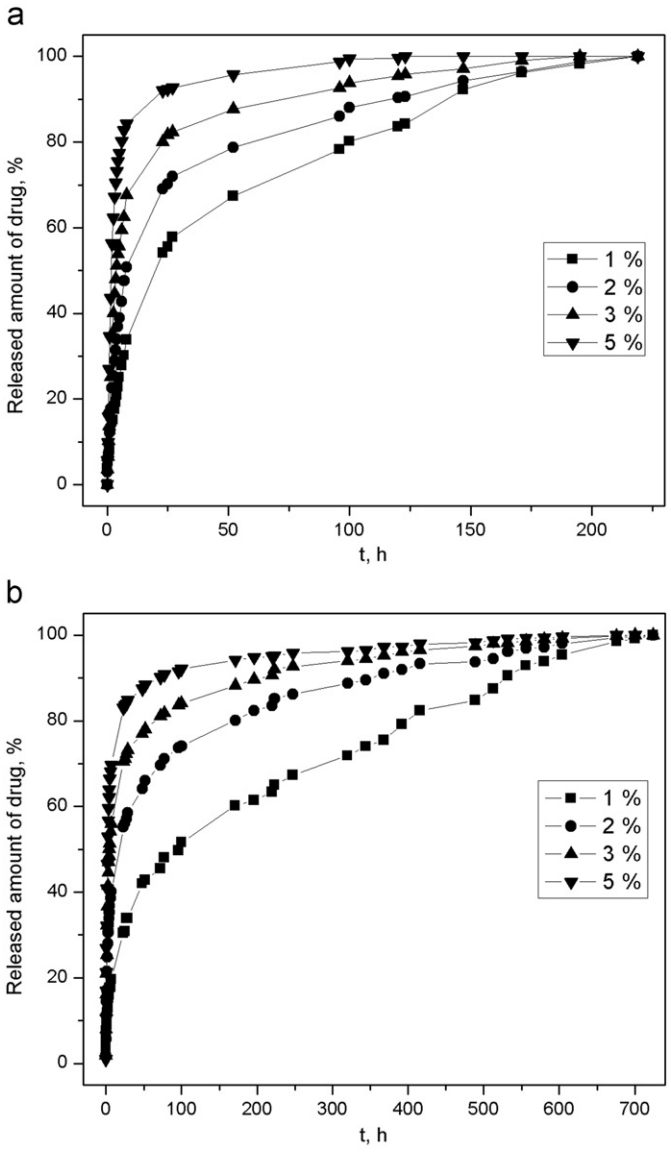

Fig. 6. Release profile of tigecycline from the tablets compressed with the pressure of: (a) 16 MPa ($SD_{1\%}$=34.127, $SD_{2\%}$=34.048, $SD_{3\%}$=33.700, $SD_{5\%}$=32.433, n=29), (b) 160 MPa ($SD_{1\%}$=32.485, $SD_{2\%}$=31.625, $SD_{3\%}$=29.745, $SD_{5\%}$=28.246; n=44).

Dependence of the determined effective diffusion coefficients (D) of the pore size distribution and drug concentration was particularly analyzed from the aspect of their influence to the coefficient value. For better insight, this dependence is presented as-log D vs. drug concentration, for various groups of pores (Fig. 8). As it can be seen, D increases with the increase of drug concentration, but it also increases with the increase of pore size, within one observed concentration.

The best way to express the rate of change of D with concentration is to analyze the ratio between D for the tablets with higher drug concentration (2, 3 and 5%) and D for the tablet with the lowest drug concentration (1%) (Fig. 9). The obtained data show that these changes are

particularly pronounced for the biggest pores, while for smaller pores, they become less and less.

On the other hand, the ratio between D for the largest and for the smallest pores (Fig. 10) increases with the increase of concentration and this is particularly pronounced for the tablets with smaller pores.

The best way to show the influence of pore size distribution and drug concentration on D was to find: (i) the ratio between D belonging to each concentration and to the lowest concentration, for constant pore value (Fig. 9) and (ii) the ratio between D for the largest pores and D for the smallest pores, for constant concentration (Fig. 10).

Comparing the values of the ratios between D for concentrations of 2, 3 and 5% (D_2, D_3 and D_5) and D for concentration of 1% (D_1), presented in Fig. 9, the highest values were noticed for the largest pores: (i) for tablets 1: $D_2/D_1=3.1$, $D_3/D_1=15$, $D_5/D_1=28$; and (ii) for tablets 2: $D_2/D_1=9.2$, $D_3/D_1=30$, $D_5/D_1=52$.

On the other hand, comparing the ratios between D for the largest pores and for the smallest pores, for drug concentrations of 1, 2, 3 and 5%, the following values were obtained: (i) 10, 68, 236 and 300 respectively, for tablets 1 and (ii) 27, 139, 450 and 636, respectively, for tablets 2.

The highest observed values of the ratio between D for the highest and D for the lowest concentration were observed for the largest pores: $D_5/D_1=28$ (tablet 1) and $D_5/D_1=52$ (tablet 2) while the highest values of the ratios between D for the largest pores and for the smallest pores, were noticed for the highest concentration: 300 (tablet 1) and 636 (tablet 2). These data show that values obtained for the constant concentration are more than ten times higher than values obtained for the constant pore size. Therefore, it follows that pore size has a dominant influence on the value of diffusion coefficient (the drug concentration has impact roughly 10%, while pore size distribution has impact of about 90%).

Applying the Korsmeyer–Peppas (KP) equation, in logarithmic form, to data related to the release from both tablets, it was confirmed that this equation can be applied for the initial period of release only (when about 60% of the total drug quantity was released), except for tablet 2 and the drug concentration of 1%, when it fits the experimental data over the whole period of drug release (Fig. 11).

As hydroxyapatite used for fabrication of tablets has a very complex structure (agglomerates (1–5 μm), particles (200 nm), subparticles (160 nm), crystallites (8–22 nm)), it was necessary to examine the correlation between the drug

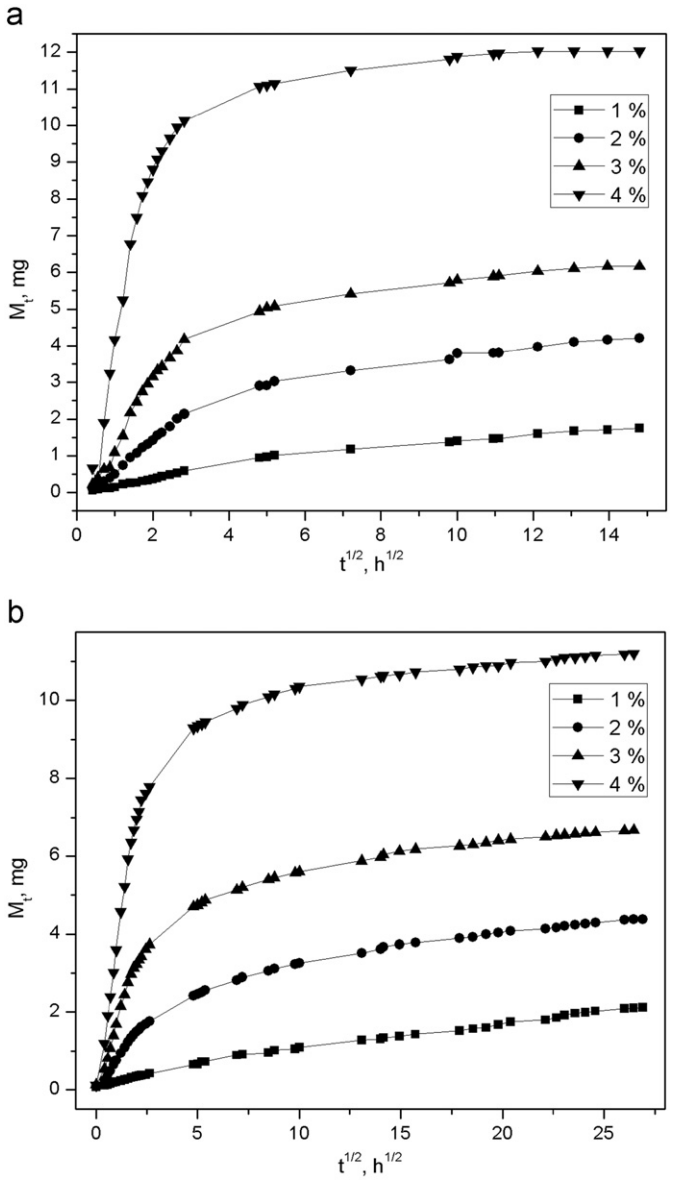

Fig. 7. Fitting data by Higuchi's equation, for: (a) tablets 1 ($SD_{1\%}=0.595$, $SD_{2\%}=1.438$, $SD_{3\%}=2.088$, $SD_{5\%}=3.965$, $n=29$), (b) tablets 2 (M_t: $SD_1=0.689$, $SD_{2\%}=1.387$, $SD_{3\%}=1.981$, $SD_{5\%}=3.166$, $n=44$).

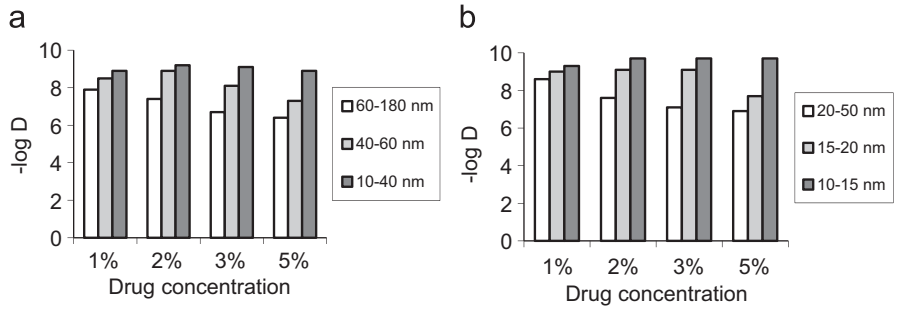

Fig. 8. Dependence of diffusion coefficient of drug concentration, for different pore groups, for: (a) tablets 1, (b) tablets 2.

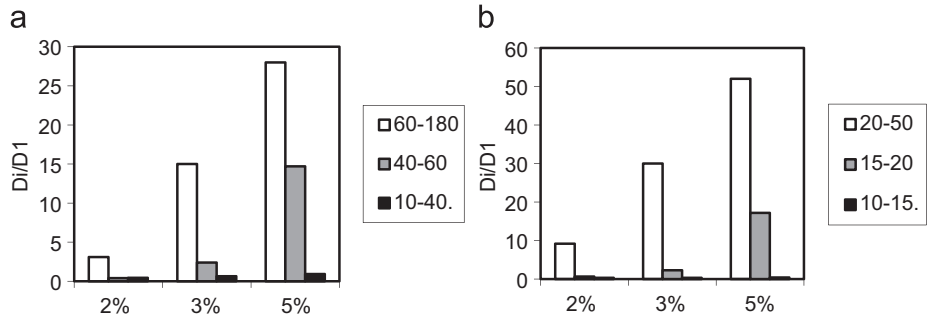

Fig. 9. Ratio between D belonging to higher drug concentrations (2, 3 and 5%) and D belonging to the lowest drug concentration (1%), for: (a) tablets 1, (b) tablets 2.

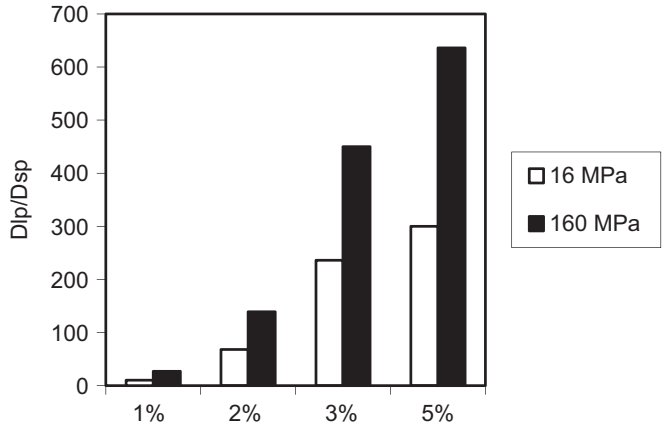

Fig. 10. Dependence of ratio between diffusion coefficients for the largest (D_{lp}) and the smallest (D_{sp}) pores on drug concentration, for the tablets compressed with the pressure of 16 and 160 MPa.

release and corresponding geometry of apatite particles. Accordingly, the relationship between the hierarchical porosity of tablets and the drug release rate was carefully analyzed, because this might be useful for designing of various delivery systems with optimal geometry.

Observing the tablet porosity data, presented in Fig. 5, it was noticed that they can be easily correlated with the corresponding drug release rates interpreted by KP model, given in Fig. 11.

If we analyze separately release from the various pores, large, medium and small, then the release kinetics can be described more preciously. Accordingly, the drug release curve for each tablet (Fig. 11) can be divided into several linear segments for which KP equation shows linear fit. Each of these segments can be characterized with the particular release exponent (coefficient of direction of the linear segment), assigned to the corresponding drug release rate. The number of segments varies depending on the drug concentration. It is almost the same for both types of tablets: for tablets with drug concentration of 2% there are three linear segments, and for concentration of 3 and 5%, there are four segments. The only difference is for the concentration of 1%, when for the tablet 1, two linear segments are observed, while for tablet 2, KP equation fits all the data.

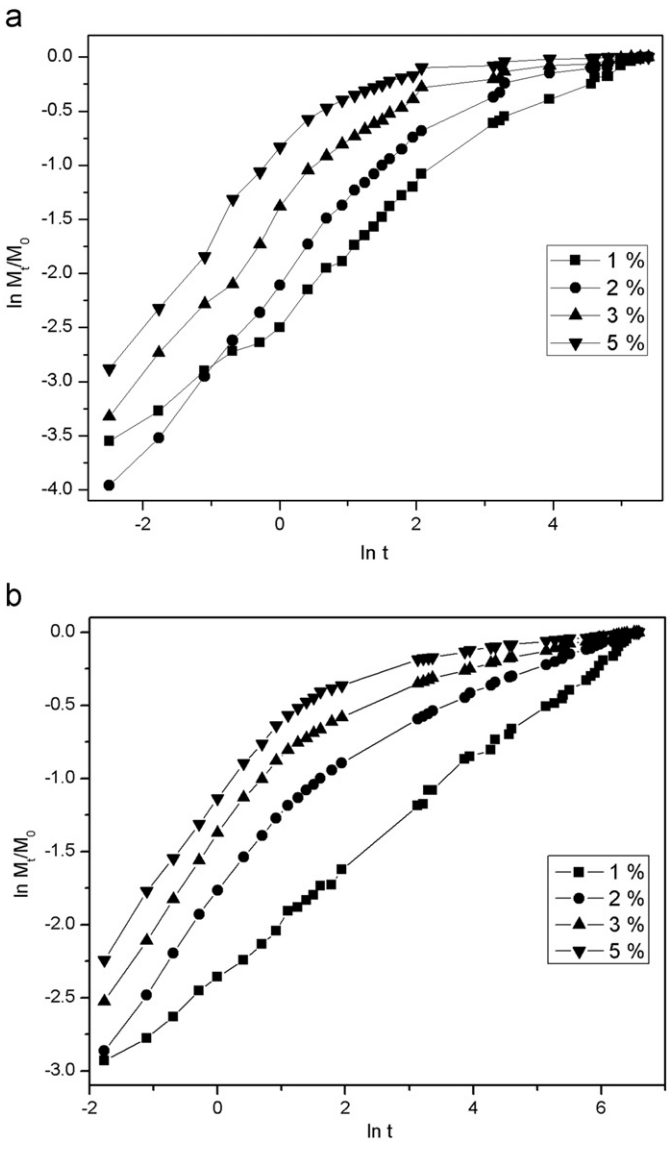

Fig. 11. Fitting data by Korsmeyer–Peppas model, for: (a) tablets 1 ($SD_{1\%}=1.075$, $SD_{2\%}=1.118$, $SD_{3\%}=0.895$, $SD_{5\%}=0.738$, $n=29$), (b) tablets 2 ($SD_{1\%}=0.892$, $SD_{2\%}=0.732$, $SD_{3\%}=0.609$, $SD_{5\%}=0.522$, $n=44$).

For the tablet 1 (Fig. 11a) and drug concentration of 1% there are two linear segments, with release exponents of 0.5 and 0.27. First of them covers the period of 27 h when

58% of drug was released, what can be related to the release from the pores 70–180 nm (50% of the total pore volume). The second covers the period of 192 h and the quantity of drug released (42%) can be associated with the pores 10–70 nm in diameter (50% of the total pore volume).

For the concentration of 2% there are three linear segments. The release is the fastest in the initial stage (exponent $n=0.73$) and is related to the largest pores (70–180 nm, 50% of the total pore volume). During this period (8 h), the amount of drug released was approximately 51%. During the next 15 h, the drug release rate is lower ($n=0.3$). The quantity of drug released (about 18%) can be associated with the pores 60–70 nm (21% of the total pore volume). And finally, the last linear segment, which covers the period of 196 h, shows the lowest release rate ($n=0.16$). During this time 31% of the total drug quantity was released, which can be associated with the release from the smallest pores with diameters of 10–60 nm (29% of the total pore volume).

For the concentration of 3%, 51% of the drug was released within the first linear segment (4 h, $n=0.87$), what corresponds to the partition of the pores of 70–180 nm in total pore volume (50%). During the next segment (4 h, $n=0.38$) about 17% of the drug was released, which is related to the pores 60–70 nm (21%). Released amount of drug during the third segment (15 h, $n=0.16$) was 12% and is associated with the pores 50–60 nm (12%). During the last segment (172 h, $n=0.1$), the released amount of drug (20%) is related to the pores 10–50 nm (17%).

For the concentration of 5%, during the first segment (3 h, $n=0.9$) about 67% of the drug was released, which is related to the pores 60–180 nm (71%). Within the second linear segment (5 h, $n=0.23$) 17% of drug was released what can be associated with the pores 50–60 nm (12%). For the third and forth segment (15 h, $n=0.08$ and 124 h, $n=0.05$, respectively) the amount of drug released was 8%, which coincides with the partition of pores 40–50 nm (8%) and 10–40 nm (9%) in total pore volume.

For the tablet 2 (Fig. 11b) and drug concentration of 1%, as it is mentioned before, KP equation fits the experimental data over the whole period of drug release ($R^2=0.996$). The release exponent, obtained from direction coefficient, gives the value of release exponent of 0.4.

For the concentration of 2% there are three linear segments (7 h, $n=0.54$; 22 h, $n=0.24$ and 615 h, $n=0.16$, respectively). Released amounts of drug were 41, 18 and 41%, respectively, that can be related to the pores 25–50 (45%), 20–25 (19%) and 10–20 nm (36%), respectively.

For the concentration of 3% there are four linear segments (3 h, $n=0.61$; 4 h, $n=0.27$, 22 h, $n=0.19$ and 671 h, $n=0.097$, respectively). Released amounts of drug were about 45, 11, 17 and 27%, respectively, that can be related to the pores 25–50 (45%), 20–25 (19%), 17.5–20 (13.5) and 10–20 nm (22.5%), respectively.

For the concentration of 5% there are also four linear segments (3 h, $n=0.58$; 4 h, $n=0.25$, 22 h, $n=0.16$ and 671 h, $n=0.049$, respectively). Released amounts of drug were about 57, 13, 15 and 25%, respectively, that can be related to the pores 20–50 (63%), 20–17.5–20 (13.5), 15–17.5 (11.5%) and 10–15 nm (11%), respectively.

The presented data indicate that, within any linear interval, the percentage of drug released and the percentage of pores of certain sizes present in the sample is approximately the same. Thus, it follows that the geometry (porosity) is of great importance for the drug release kinetics, and therefore requires further examination.

4. Conclusions

In this study we proposed a new approach to interpreting the mechanism of drug release from ceramic materials, which determines the relationship between pore sizes and the drug release rate. Higuchi and Korsmeyer–Peppas model, applied in a modified procedure, enabled determination of relations between pore sizes, their distribution and drug release rate.

Particularly, the influence of pore size distribution and drug concentration on diffusion coefficients was studied using analytical solution of Fick's second law of diffusion. It was found that pore size has a dominant impact on the value of diffusion coefficient, roughly 90%, while the drug concentration has impact of only about 10%.

For the first time in literature, to the best of our knowledge, it has been clearly confirmed that if the porosity of any drug release device is precisely determined, then it is possible to fully predict the rate of its drug release.

Acknowledgment

This study was financially supported by the Ministry of Science and Technological Development of the Republic of Serbia (Project no. 172026).

References

[1] M.P. Ginebra, T. Traykova, J.A. Planell, Calcium phosphate cements as bone drug delivery systems: A review, Journal of Controlled Release: Official Journal of the Controlled Release Society 113 (2006) 102–110.
[2] W.J.E.M. Habraken, J.G.C. Wolke, J.A. Jansen, Ceramic composites as matrices and scaffolds for drug delivery in tissue engineering, Advanced Drug Delivery Reviews 59 (2007) 234–248.
[3] Y. Boonsongrit, H. Abe, K. Sato, M. Naito, M. Yoshimura, H. Ichikawa, Y. Fukumori, Controlled release of bovine serum albumin from hydroxyapatite microspheres for protein delivery system, Materials Science and Engineering B 148 (2008) 162–165.
[4] A.K. Jain, R. Panchagnula, Skeletal drug delivery systems, International Journal of Pharmaceutics 206 (2000) 1–12.
[5] S. Esposito, S. Leone, Prosthetic joint infections: microbiology, diagnosis, management and prevention, International Journal of Antimicrobial Agents 32 (2008) 287–293.
[6] N. Fletcher, D. Sofianos, M.B. Berkes, W.T. Obremskey, Prevention of perioperative infection, The Journal of Bone and Joint Surgery American Volume 89 (2007) 1605–160518.

[7] A. Slosarczyk, J. Szymura-Oleksiak, B. Mycek, The kinetics of pentoxifylline release from drug-loaded hydroxyapatite implants, Biomaterials 21 (2000) 1215–1221.
[8] S. Lepretre, F. Chai, J.C. Hornez, G. Vermet, C. Neut, M. Descamps, H.F. Hildebrand, B. Martel, Prolonged local antibiotics delivery from hydroxyapatite functionalized with cyclodextrin polymers, Biomaterials 30 (2009) 6086–6093.
[9] M. Teller, U. Gopp, H.G. Neumann, K.D. Kühn, Release of gentamicin from bone regenerative materials: an in vitro study, Journal of Biomedical Materials Research Part B: Applied Biomaterials 81 (2007) 23–29.
[10] N.M. Ruiz, E. Gayoso, Y. Vasquez, Tigecycline usage in osteomyelitis caused by multidrugresistent acinetobacter: A report of 10 cases from a single institution, 14th International Congress on Infectious Diseases (ICID) Abstracts, http://dx.doi.org/10.1016/j.ijid.2010.02.1932.
[11] R. Haidar, A. Der Boghossian, B. Atiyeh, Duration of post-surgical antibiotics in chronic osteomyelitis: empiric or evidence-based?, International Journal of Infectious Diseases 14 (2010) 752–758
[12] L.Y. Yin, L. Lazzarini, F. Li, C.M. Stevens, J.H. Calhoun, Comparative evaluation of tigecycline and vancomycin, with and without rifampicin, in the treatment of methicillin resistant Staphylococcus aureus experimental osteomyelitis in a rabbit model, Journal of Antimicrobial Chemotherapy 55 (2005) 995–1002.
[13] J. Hylands, Tigecycline: A new antibiotic, Intensive and Critical Care Nursing 24 (2008) 260–263.
[14] M.P. Ginebra, T. Traykova, J.A. Planell, Calcium phosphate cements: Competitive drug carriers for the musculoskeletal system?, Biomaterials 27 (2006) 2171–2177.
[15] R.W. Korsmeyer, R. Gurney, E. Doelker, P. Buri, N.A. Peppas, Mechanisms of solute release from porous hydrophilic polymers, International Journal of Pharmaceutics 15 (1983) 25–35.
[16] A.K. Jena, M.C. Chaturvedi, Phase Transformations in Materials, Prentice Hall, 1992, p. 247.
[17] H. van de Belt, D. Neut, D.R.A. Uges, W. Schenk, J.R. van Horn, H.C. van der Mei, H.J. Busscher, Surface roughness, porosity and wettability of gentamicin-loaded bone cements and their antibiotic release, Biomaterials 21 (2000) 1981–1987.
[18] M. Espanol, R.A. Perez, E.B. Montufar, C. Marichal, A. Sacco, M.P. Ginebra, Intrinsic porosity of calcium phosphate cements and its significance for drug delivery and tissue engineering applications, Acta Biomaterialia 5 (2009) 2752–2762.
[19] A. Cosijns, C. Vervaet, J. Luyten, S. Mullens, F. Siepmann, L. Van Hoorebeke, B. Masschaele, V. Cnudde, J.P. Remon, Porous hydroxyapatite tablets as carriers for low-dosed drugs, European Journal of Pharmaceutics and Biopharmaceutics 67 (2007) 498–506.
[20] M. Oner, E. Yetiz, E. Ay, U. Uysal, Ibuprofen release from porous hydroxyapatite tablets, Ceramics International 37 (2011) 2117–2125.
[21] V. Jokanović, D. Izvonar, M.D. Dramićanin, B. Jokanović, V. Živojinović, D. Marković, B. Dačić, Hydrothermal synthesis and nanostructure of carbonated calcium hydroxyapatite, Journal of Materials Science: Materials in Medicine 17 (2006) 539–546.
[22] M.Y. Nakahigashi, Y. Matsuda, J.L. Fox, W.I. Higuchi, Y. Sugiyama, Effect of geometrical cement size on in vitro and in vivo indomethacin release from self-setting apatite cement, Journal of Controlled Release 52 (1998) 281–289.
[23] Q. Xu, Y. Tanaka, J.T. Czernuszka, Encapsulation and release of a hydrophobic drug from hydroxyapatite coated liposomes, Biomaterials 28 (2007) 2687–2694.
[24] A. Lebugle, A. Rodrigues, P. Bonnevialle, J.J. Voigt, P. Canal, F. Rodriguez, Study of implantable calcium phosphate systems for the slow release of methotrexate, Biomaterials 23 (2002) 3517–3522.
[25] P. Liu, T. Ju, Y. Qiu, Diffusion-Controlled Drug Delivery Systems, in: X. Li, B.R. Jasti (Eds.), Design of Controlled Release Drug Delivery Systems, McGraw-Hill, USA, 2006, pp. 107–137.
[26] A. Akashi, Y. Matsuya, M. Unemori, A. Akamine, Release profile of antimicrobial agents from α-tricalcium phosphate cement, Biomaterials 22 (2001) 2713–2717.